An approach for quantitative EHD friction prediction based on rheological experiments and molecular dynamics simulations

Ruibin Xu[1], Laetitia Martinie[1], Philippe Vergne[1], Laurent Joly[2], and Nicolas Fillot[1,*]

[1]Univ Lyon, INSA Lyon, CNRS, LaMCoS-UMR5259, Villeurbanne F-69621, France

[2]Univ Lyon, Univ Claude Bernard Lyon 1, CNRS, Institut Lumière Matière, F-69622, Villeurbanne, France

[*]Corresponding author nicolas.fillot@insa-lyon.fr

Abstract

Lubricated friction is controlled by the contact operating conditions, including temperature, normal load and sliding. In the elastohydrodynamic (EHD) regime, the rheological characteristics of the lubricants are also dependent on these conditions. Under extreme contact conditions (high load, high sliding), a possible friction plateau (limiting shear stress phenomena) can appear, making friction independent of the sliding speed. Since the physical origin of this friction plateau remains unclear, despite many efforts from the tribology community, predicting friction in EHD contact is still challenging. This work introduces an original EHD friction prediction approach built on a completely independent process from the tribological test. It consists of implementing two models a viscosity model based on the rheological experiment and molecular dynamics simulation data combined with a thermal-elastohydrodynamic contact model. Two fluids with different natures are studied squalane and benzyl benzoate. Friction predictions, including friction plateau and thermal effects, are obtained for both fluids and compared with experimental friction measurements, and a quantitative agreement is obtained. In addition, the role of the thermal effects on EHD friction and the origin of the friction plateau are investigated.

Keywords

EHD friction, limiting shear stress (LSS), Eyring model, molecular dynamics (MD) simulations

1 Introduction

Energy losses due to friction make up to one-third of the total energy losses in engineering applications [1]. Friction is typically quantified by the friction coefficient C_f, defined as the ratio between the tangential force F_T as opposed to the sliding and the normal applied load F_N.

$$C_f = \frac{F_T}{F_N} \tag{2}$$

The prediction of friction has long been a dream of the tribology community, as it also represents a real need of the industry. First, being able to predict friction reflects a full understanding of its underlying mechanism. Additionally, the industry needs to predict friction to optimise energy losses in mechanical components and structures to improve their performance and durability. This study focuses on friction prediction in EHD (elastohydrodynamic) lubrication, a typical example being the contacts in bearings or gears, where pressures classically go up to 3GPa. Due to elastic deformations of the surfaces, the contact zone is a narrow gap between two almost parallel surfaces, separated by a (typically) 100nm thick film. The mean shear rate $\dot{\gamma}$, estimated as the ratio between the sliding velocity Δu and the lubricant film thickness h_c measured at the centre of the contact, ranges typically from $10^4 s^{-1}$ to $10^7 s^{-1}$.

$$\dot{\gamma} = \frac{\Delta u}{h_c} \tag{2}$$

Under such extreme conditions, friction successively experiences several different regimes, these regimes can be identified in figure 1 exhibiting the friction coefficient variation versus the slide-to-roll-ratio (SRR). $SRR = \frac{u_e}{\Delta u}$ is defined as the ration between the entrainment velocity $u_e = \frac{u_1+u_2}{2}$ and the sliding velocity $\Delta u = u_1 - u_2$. First, a linear regime where friction increases linearly with $\dot{\gamma}$; second, a non-linear (shear thinning) regime where friction departs from its initial linear behaviour, which is often attributed to the shear thinning effect; and finally, at very high shear rates, a thermoviscous regime where shear heating decreases fluid viscosity and reduces friction. However, under certain conditions, friction saturates and presents a plateau, becoming independent of $\dot{\gamma}$.

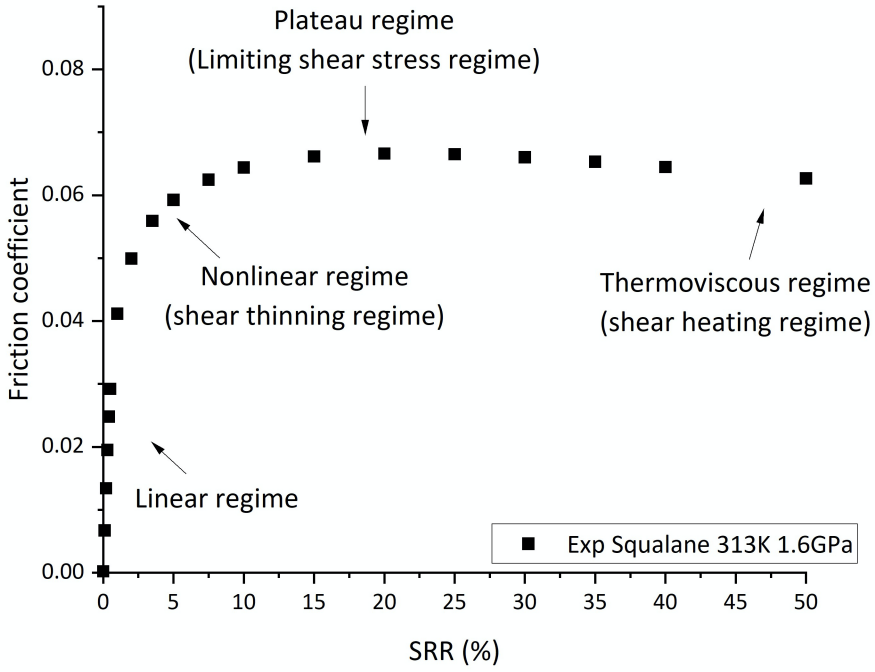


Figure 1: Typical EHD friction curve, data from the present study.

Contrary to the piezo-viscous response of lubricants, which is extensively studied in the literature [2, 3, 4], little is known about the plateau regime at high pressure. In this regime, the friction coefficient, associated in the literature with the limiting shear stress (LSS), becomes shear rate independent. LSS was first described by Smith [5] in the 1960s, but till now, the multi-physics nature of the contact problem has made it impossible to reach a consensus on its physical origin [6]. Some researchers believe that the LSS is generated by local kinematic characteristics in the fluid, such as wall slip [7], shear localisation [8] and plug flow [9]. However, the severe conditions inside a contact (high confinement and high shear rates) strongly limit the in-situ measurements that can be performed. Thus, the local kinematic assumption remains unproven. For others, the LSS is an inherent material property. This idea was first suggested by Bair and Winer [10]. More evidence has supported it in recent years studies such as Muraki et al. [11], and Tsubouchi et al. [12] found that molecular structure has an impact on EHD (elastohydrodynamic) friction. Based on these findings, Zhang et al. [13] carried out a series of tribological experiments on different fluids. Results indicated that under isothermal operating

conditions, all traction fluids reached their limiting values while the low friction base oils (lubricants) did not. They thus concluded that friction in EHD lubrication regime is significantly influenced by the molecular structure of the base fluid. In another subsequent paper, Ewen et al. [14] confirmed the conclusion of Zhang et al. [13] through molecular dynamics simulations.

On the other hand, Ndiaye [15] suggested that the LSS phenomenon only occurs above the glass transition pressure of the fluid [16]. In a subsequent study of highly loaded contacts, Ndiaye et al. [17] correlated friction plateau's onset with the lubricant's glass transition. This correlation was later confirmed by Porras-Vazquez et al. [18], who compared both tribological tests and molecular dynamics simulations on squalane and benzyl benzoate. The results show that for both fluids in the liquid state, no LSS plateau was found, whereas for squalane and benzyl benzoate in the solid-like state, the LSS plateau was observed both in simulations and experiments. They thus concluded that the thermodynamic state of the lubricant in the contact area is the key to understanding the origin of LSS.

For the prediction of friction, the first requirement is to accurately characterise the rheological properties of lubricants. In some early works [19], researchers tried to do so by using apparent viscosity derived from tribological tests. With more accurate friction measurements obtained, they turned to directly characterising friction by fitting equations to traction curves, such as the Johnson and Tevaarwerk equation [20]. This model was later accepted by researchers and further refined to fit the experimental results better and account for the temperature rise and pressure distribution in contact [8, 21]. Based on these characterisations, numerous empirical prediction methods have emerged. Among them are, sophisticated numerical methods such as those by Jacod et al. [22, 23] and also some simple analytical tools for engineering purposes such as Olver and Spikes [24] and Morales-Espejel and Wemekamp [25]. Despite all these efforts, such methods use data derived from tribological experiments to reproduce the friction value of the same experiments. Since such methods work a posteriori, their use is limited to a given set of operational conditions, making it impossible to transfer them to other conditions or lubricants.

Significant progress has been made in friction prediction since the breakthrough in high-pressure viscometer technology for measuring the rheological properties of bulk fluid. These contact independent data collected in the range of pressure and temperature experienced in a lubricated contact enable a proper friction prediction. Using these data, researchers have successfully predicted

EHD friction for both isothermal [26, 27, 28, 29] and thermal environments [30]. These pioneering works have inspired many subsequent studies of thermal EHD contact, such as Doki-Thonon [31], Wheeler [32], Liu et al. [33], and Björling et al.[34]. Despite the quality of the obtained results, one typical drawback of these predictions is the inability to account for limiting shear stress without using an empirical LSS model derived from tribological tests [23, 24, 25, 26, 27, 29, 30, 33, 34, 35] which prevents them from being true, independent from friction experiment, predictions.

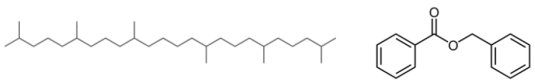
This study proposes a new EHD friction prediction approach at the contact scale. A finite element method (FEM) is used to solve the Reynolds equation and the equations capturing other physical phenomena (such as non-Newtonian and thermal effects) to predict friction. This method has been referred to as 'full numerical simulation' to distinguish it from other simplified methods [33]. It also requires an accurate constitutive law of the rheology of the fluid. This law is chosen in such a way as to be able to predict friction plateau while being derived from contact-independent data, such as viscosity measured in high-pressure viscometers. For those parts that lack the support of experimental methods, molecular dynamics simulations are used.

The rheological properties used in the present approach and the reasoning behind their selection are shown in the methodology in section 2. It is followed by the presentation of characterisation tools and the FEM contact model in section 3. In section 4, characterisation results and corresponding friction prediction results are presented and discussed.

2 Methodology

2.1 Choice of fluids

The proposed approach in this paper is applied to two fluids chosen for their different tribological behaviour. Squalane (SQ) is a linear n-alkane with formula $C_{30}H_{62}$, having an elongated and flexible structure while also being a reference lubricant in EHD lubrication research [36]. Secondly, benzyl benzoate (BB) is an organic compound which is the ester of benzyl alcohol and benzoic acid with the formula $C_6H_5COOCH_2C_6H_5$. It has a bulky and more compact structure (figure 2(b)) as opposed to SQ (figure 2(a)). Both fluids have already been explored experimentally [28, 37, 38] and with MD simulations [39, 40, 41, 42] concerning their frictional and rheological properties.



(a) (b)

Figure 2: Molecular structures of the fluids investigated (a) SQ and (b) BB.

2.2 Rheological model

a Non-Newtonian viscosity model

Debate on the best rheological model to properly describe the EHD lubrication regime has long revolved around two families of models [19, 43] Eyring and Carreau. Both models are widely used in EHD friction research; as seen in [26, 27, 28, 30, 33] for Carreau and [23, 24, 25] for Eyring.

On the one hand, Carreau [44] suggested a power-law model describing the viscosity-shear rate dependency in 1972. This model was later improved by Yasuda et al. [45], and finally, it was Bair [46] who generalised it and made it more suitable for EHD solvers. This Carreau-Yasuda-Bair law relates the generalised viscosity η and shear stress τ, and is written as equation 3.

$$\eta = \frac{\eta_N}{\left[1 + \left(\frac{\tau}{G}\right)^a\right]^{\left(\frac{1}{n} - 1\right)/a}} \tag{3}$$

where η_N is the Newtonian viscosity, a and n are two constant parameters, G is a critical shear stress of the Newtonian regime.

On the other hand, Eyring published a rheological model based on the stress-augmented-thermal-activation (SATA) concept in 1936 [47], as shown in equation 4.

$$\eta = \frac{\tau_e}{\dot{\gamma}} \sinh^{-1}\left(\frac{\eta_N \dot{\gamma}}{\tau_e}\right) \tag{4a}$$

$$\tau = \tau_e \sinh^{-1}\left(\frac{\eta_N \dot{\gamma}}{\tau_e}\right) \tag{4b}$$

The τ_e is called the Eyring stress, which describes the shear stress threshold required for significant shear thinning to occur, similar to G in the Carreau model. Eyring model assumes that the viscous flow

originates from the motion of molecules from one equilibrium position to another, and this process requires crossing an energy barrier with the help of thermal activation. In the presence of shear, the energy barrier is lowered in the direction of shear to favour molecular motion.

Both models require the characterisation of fluid properties. However, the Eyring model has only two parameters the Newtonian viscosity η_N and the Eyring stress τ_e. Compared to the Carreau model, which has four parameters, this simplicity greatly facilitated the characterisation process.

Jadhao and Robbins [39, 40] carried out a series of studies on the rheological properties of SQ using non-equilibrium molecular dynamic (NEMD) simulations. They found that the Eyring model was able to describe the reduced viscosity $\eta_{red.} = \eta/\eta_N$ of SQ up to 30 orders of magnitude of the reduced shear rates $\dot{\gamma}_{red.} = \dot{\gamma}/\dot{\gamma}_c$. The $\dot{\gamma}_c$ is known as the critical shear rate, which represents the shear rate threshold for significant shear thinning to occur. It is usually associated with the relaxation time t_{rel} of fluid via $\dot{\gamma}_c = 1/t_{rel}$. Meanwhile, the Carreau model failed to reproduce the variation in shear thinning rate over the same range. This implied a better versatility of the Eyring model for EHD lubrication problems since t_{rel} and $\dot{\gamma}_{red.}$ vary due to drastically changing conditions in EHD contact where the pressure goes from zero to a few Giga pascals in the contact area.

For these reasons, the Eyring model is chosen as the rheological model in the present study. Thus its parameters need to be determined. In fact, the controversy over Carreau and Eyring model lies mainly in whether traction curves can be used to characterise the rheological behaviour of fluids. Indeed, the Eyring model was first used to fit the mean shear stress versus the mean shear rate derived from traction curves to obtain the rheological characteristics, as was done by Johnson and Tevaarweak [20]. However, in a recent article, Bair [48] points out that the traction curve is not a flow curve and that the response of fluids to shear rate is not the same as the relationship between mean shear stress and mean shear rate obtained from traction curves. The authors similarly endorse this view. Therefore in the present approach, the parameters of the Eyring model are determined contact-independently. Rheological measurements under pressure provided a basis for first characterising the viscosity-pressure dependence and then estimating it over larger ranges using a correlation that is more accurate than free volume-based models and thus of course more accurate than the empirical models used in classical

EHD. Because the Eyring stress τ_e is not yet reachable with the experiment, it is characterised with the help of NEMD simulations. The rheological model is then implemented in a thermal EHD contact model to predict friction. Details are presented in section 2.4.

b Density and Newtonian viscosity model

The Tait equation of state widely described in the literature [49] is implemented in the contact model to link the relative volume to the pressure and temperature of both fluids. The density ρ is then derived from this equation via the reference density ρ_R measured at atmosphere pressure p_{atm} and the reference temperature T_R, this is shown in equation 5.

$$\frac{V}{V_R} = [1 + a_v (T - T_R)] \times \left[1 - \frac{1}{1 + K_0'} \ln\left(1 + \frac{p}{K_0}(1 + K_0')\right)\right]$$
$$\frac{V}{V_R} = \frac{\rho_R}{\rho} \tag{5}$$

where $K_0 = K_{00}\, exp(-\beta_k T)$, and K'_0, a_v, K_{00} and β_k are the parameters of the Tait equation of state given in table 1. The parameters for SQ are taken from Bair [36], and the reference density is taken from Mylona et al. [50]. The parameters for BB are derived from the results of the same test as SQ performed by Bair [51], and the reference density of BB is measured at LaMCoS - INSA de Lyon with a density meter DMA4500M from Anton Paar.

	K_0'	a_v[K^{-1}]	K_{00}[GPa]	β_K[K^{-1}]	ρ_R[kg/m^3] at 313.15K
SQ[36]	11.74	8.36×10^{-4}	8.658	6.332×10^{-3}	795.8[50]
BB[51]	10.44	7.47×10^{-4}	13.707	6.107×10^{-3}	1102.3[This study]

Table 1: Parameters of Tait equation of state and density measurements for SQ and BB.

The thermal scaling law of Bair and Laesecke [35], already successfully applied to the SQ, has been used in the present study. It has the crucial advantage of accurately reproducing the viscosity-pressure dependence on large high-pressure scales, which is not the case for the classical models (Barus, Roelands...) used in most of the EHD lubrication models. Here, the Newtonian viscosity η_N is expressed through a thermal scaling parameter φ as $\eta_N = f(\varphi)$ with φ commonly written as equation 6.

$$\varphi = \left(\frac{T}{T_R}\right)\left(\frac{V}{V_R}\right)^g \tag{6}$$

And $f(\varphi)$ a normalised Ashurst-Hoover equation written as equation 7.

$$\eta_N = A\exp\left(B\varphi^{-q} + C\varphi^{-Q}\right), \qquad 0 < q < 1, \qquad 1 < Q \tag{7}$$

Adjusting the viscosity law equation 7 on the experimental data of viscosity from Bair [36] for the SQ and from Ndiaye et al. [37] for the BB led to the fitting parameters given in table 2. As seen in figure 3, squalane shows a slower-than-exponential increase in viscosity with pressure up to about 1GPa, above which the viscosity increases faster-than-exponential. On the other hand, benzyl benzoate viscosity increases faster-than-exponential over most of the pressures studied. The results show a standard deviation of 10.77% from the experimental measurements for SQ and 4.13% for BB, which cover 7 and 4 decades of viscosity respectively.

	A[Pa.s]	B[K]	C[K]	q	Q	g
SQ[This study]	3.531×10^{-5}	6.016	0.133	0.999	3.954	3.521
BB[This study]	6.807×10^{-5}	4.280	0.155	0.871	6.037	4.569

Table 2: Parameters of the Newtonian viscosity law of SQ and BB.

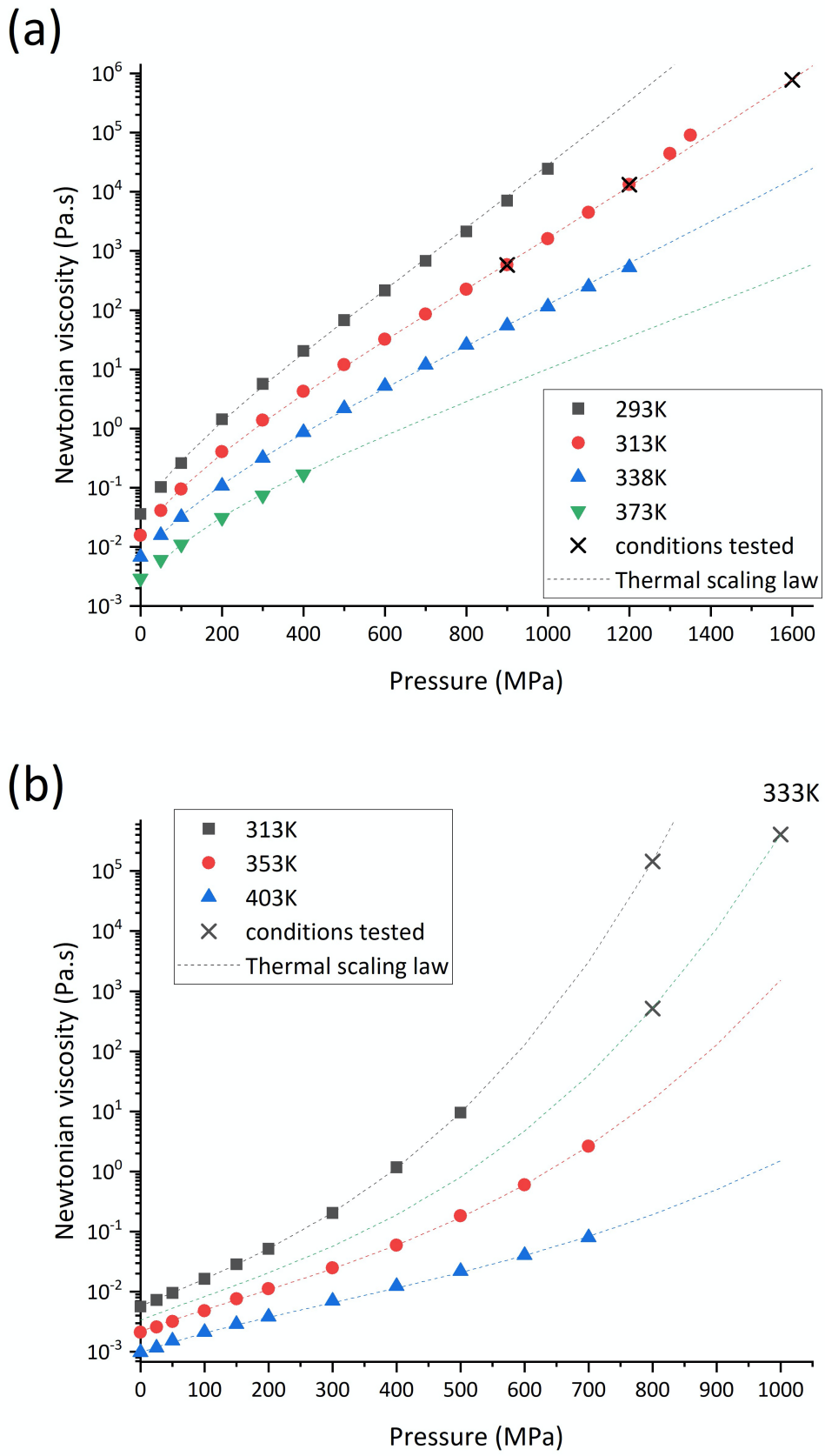


Figure 3: Comparison between viscosity measurements (filled symbols) and the thermal scaling law predictions (dash lines). (a) SQ, experimental data from [36]. (b) BB, experimental data from[37]. The operating conditions for the friction experiments of the present study are marked as black crosses.

2.3 Non-equilibrium molecular dynamics simulations

The previous study from Jadhao and Robbins [39, 40] led to deriving Eyring stress from MD simulations. They performed NEMD simulations on bulk SQ using the SLLOD algorithm [52] with LAMMPS [54]. A Nosé-Hoover thermostat [55] was used to control the temperature. They found that the shear stress of SQ increases logarithmically with the shear rate at a high rate, following Eyring's model. They derived the Eyring stress from the slope of shear stress versus shear rate curve and exhibited its independence from pressure for T>250K and p>300MPa.

Meanwhile, others performed confined NEMD simulations at constant pressure, which is consistent with tribology experiments, following the methodology described in Ewen et al.[14] and Porras-Vazquez et al. [18]. Both studies showed a good correlation between the experimental friction curve and NEMD simulation results at the molecular scale. The present study uses confined NEMD to determine the Eyring stress. SQ is first tested to validate our approach by comparing obtained results with those from the literature [14, 40]. The BB is then tested to determine its Eyring stress under different operating conditions. Results are presented in section3.

All molecular systems in this study have been built using the open-source LAMMPS builder program [56], which uses modules from Moltemplate [58], and ASE [59]. The confined system (see figure 4) contains two rough FeO surfaces and 720 SQ molecules or 1440 BB molecules between them. Periodic boundary conditions are imposed in the x and y directions. The dimensions of the solid surface are approximately 5nm×5nm (in x and y directions) and have a thickness from 3nm to 5nm (in z direction). The dimensions of the simulation boxes were chosen to be big enough to ensure they do not affect the results. The roughness of the contact walls is generated by a self-affine fractal scaling law [14], where the Hurst exponent is set to 0.8 [60], and the root mean square (RMS) roughness is set to 0.8 nm. The contact surface is described with the classical empirical EAM force field [61], which is widely used in metallic systems. The interaction within fluid molecules includes both Lennard-Jones and Coulomb potentials. It is described by the L-OPLS-AA force field [62]. This force field has previously been used in the simulations of many lubricants, including SQ [14, 18] and traction fluids, including BB [18]. The simulation process has three stages equilibration, compression, and shear. The energy of the system is first minimised. The system was then equilibrated using a Nosé-Hoover thermostat with a damping coefficient of 0.1ps, applied to the whole system in the y direction only to avoid affecting the shearing in the x direction and the pressure in the z direction. This stage runs for 0.5ns to randomise the positions of fluid molecules (5×10^5 time steps). In the compression stage, a constant pressure is applied on the upper surface with the same thermostat used to control temperature, running for 2ns (2×10^6 time steps). Finally, in the shear stage, velocity is applied on each solid surface to create shear. This stage runs for as long as possible to obtain the best signal-to-noise ratio. In the actual numerical process, the simulation time was set to at least 5ns for SQ and 8ns for BB (5×10^6 and 8×10^6 time steps). The velocity profile of the last 2 ns (2 ×

10^6 time steps) of each result was traced to check if the steady state had been reached. The resulting steady-state stress versus shear rate data in the last 2 ns were later processed to obtain the Eyring stress.

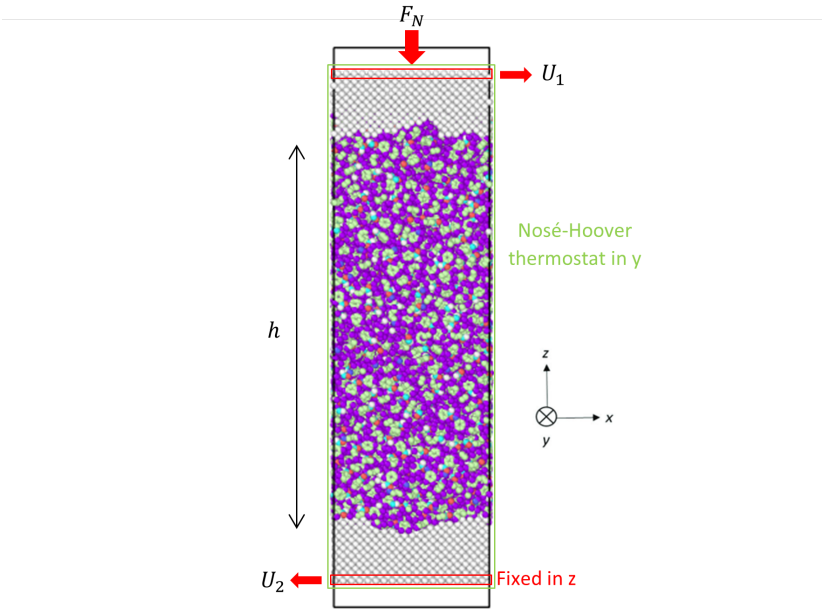


Figure 4: Confined NEMD system used in this study, taking BB as an example.

2.4 EHD contact model

Habchi et al. [30], Doki-Thonon [31], Wheeler [32], and others developed a Thermal EHD non-Newtonian (TEHDnN) contact model based on the finite element method to simultaneously solve four fully coupled equations: the generalised Reynolds equation, the elastic deformation equation, the load balance equation and the heat equations in both solids and the fluid. The generalised Reynolds equation for steady-state thermal EHD point contact with non- Newtonian lubricant is given by Yang et al. [63].

$$\frac{\partial}{\partial x}\left[\left(\frac{\rho}{\eta}\right)_e \frac{\partial p}{\partial x}\right] + \frac{\partial}{\partial y}\left[\left(\frac{\rho}{\eta}\right)_e \frac{\partial p}{\partial y}\right] - \frac{\partial}{\partial x}\left(\rho_x^*\right) = 0 \tag{8}$$

where x and y directions are in the contact plane and z direction in the film thickness *h*. Compared to the classical version, the generalised Reynolds equation considers the variation of fluid properties inside the lubricant film through the operator $(\frac{\eta}{\rho})_e$ as shown in equation 9.

$$\left(\frac{\rho}{\eta}\right)_e = \frac{\eta_e}{\eta_e'}\rho_e' - \rho_e''$$
$$\rho_x^* = \rho_e'\eta_e u_m - \rho_e u_b \tag{9}$$

The average velocity $u_m = (u_t + u_b)/2$ is defined with u_t and u_b, being the velocity of the top surface and bottom surface, respectively. The variation of fluid properties across the film thickness is shown in equation 10.

$$\rho_e = \int_0^h \rho dz$$

$$\rho_e' = \int_0^h \rho \left(\int_0^z \frac{1}{\eta} dz' \right) dz \qquad \rho_e'' = \int_0^h \rho \left(\int_0^z \frac{z'}{\eta} dz' \right) dz$$

$$\frac{1}{\eta_e} = \int_0^h \frac{1}{\eta} dz \qquad \frac{1}{\eta_e'} = \int_0^h \frac{z}{\eta} dz \tag{10}$$

where $\eta(x,y,z)$ is the viscosity described by the Eyring model (see equation 4a), which depends on pressure, temperature and shear stress (or shear rate). It is based on the thermal scaling Newtonian viscosity model (see equation 7) adjusted from rheological measurements and the Eyring stress models derived from NEMD simulations, which are presented in the next section. The density $\rho(x,y,z)$ is described by the Tait equation of state (see equation 5). The Reynolds equation is solved only in a 2D region $\partial\Omega_c$, which represents the contact area, which is a boundary of a 3D solid Ω, as seen in figure 5(a). The boundary conditions for the Reynolds equation are zero pressure at the edges of the Reynolds area $\partial\Omega_c$. The viscosity $\eta(x,y,z)$ and the density $\rho(x,y,z)$ are transformed into 2D space values $\eta_e(x,y)$, $\eta_e'(x,y)$, $\rho_e(x,y)$, $\rho_e'(x,y)$ and $\rho_e''(x,y)$ via equation 10. These values are then used to solve the generalised Reynolds equation as shown in equation 9.

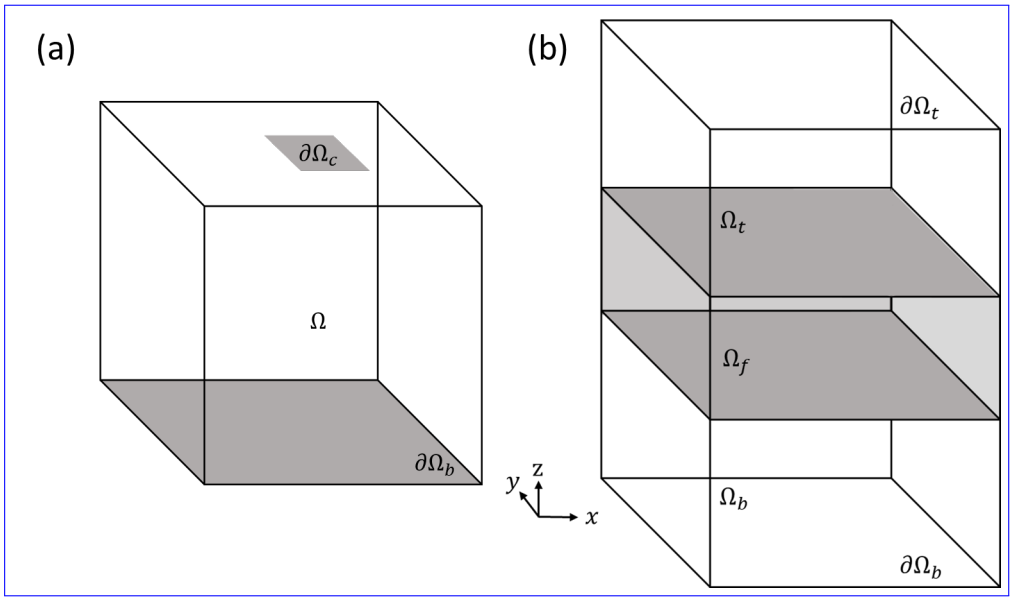


Figure 5: 3D geometry of (a) the elastic model and Reynolds area, and (b) the thermal model.

The film thickness is given by equation 11.

$$h(x,y) = h_0 + \frac{x^2 + y^2}{2R} + \delta(x,y) \tag{11}$$

where R is the radius of the equivalent solid, and h_0 represents the spacing between the two initial undeformed geometry, determined by solving the load balance equation. The load balance equation (equation 12) relates the generated pressure in the lubricant with the normal load W.

$$\iint_S p(x,y)dxdy = W \tag{12}$$

The third term $\delta(x,y)$ refers to the normal elastic deformation of the contacting surfaces, which is obtained by solving the linear elasticity equation (equation 13) in solids.

$$\nabla \cdot \sigma(u,v,w) = 0 \tag{13}$$

where σ (u,v,w) are the solid displacements in x, y, z directions respectively, and $\delta(x,y) = w(x,y,z)$ the displacement at the centre of the contact area. The bottom surface $\partial\Omega_b$ (grey surface in figure 5(a)) is clamped, and the pressure p, calculated via the generalised Reynolds equation, is imposed at the Reynolds area $\partial\Omega_c$.

With the absence of motion in the y direction, the energy balance equations for top and bottom surfaces are written as equations 14.

$$\begin{aligned}
\rho_t c_t u_{tx}\frac{\partial T}{\partial x} - \frac{\partial}{\partial x}\left(k_t\frac{\partial T}{\partial x}\right) - \frac{\partial}{\partial y}\left(k_t\frac{\partial T}{\partial y}\right) - \frac{\partial}{\partial z}\left(k_t\frac{\partial T}{\partial z}\right) = 0 \\
\rho_b c_b u_{bx}\frac{\partial T}{\partial x} - \frac{\partial}{\partial x}\left(k_b\frac{\partial T}{\partial x}\right) - \frac{\partial}{\partial y}\left(k_b\frac{\partial T}{\partial y}\right) - \frac{\partial}{\partial z}\left(k_b\frac{\partial T}{\partial z}\right) = 0
\end{aligned} \tag{14}$$

They are solved within a 3D geometry, as seen in figure 5(b). Composed of the domain of Ω_t and Ω_b, which represents the upper and lower contact solids, and Ω_f, which represents the fluid.

According to ref.[31], the heat equation for the lubricant film is written as equation 15.

$$\rho_f c_f\left(u_{fx}(x,y,z)\frac{\partial T}{\partial x} + u_{fy}(x,y,z)\frac{\partial T}{\partial y}\right) - \frac{\partial}{\partial z}\left(k_f\frac{\partial T}{\partial z}\right) = Q_{comp} + Q_{shear} \tag{15}$$

Where the $u_{fx}(x,y,z)$ and $u_{fy}(x,y,z)$ represent the velocity of the fluid at any point in the lubricant film in the x and y directions. Q_{comp} and Q_{shear} represent the compression and shear heat sources, respectively, as shown in equation 16.

$$\begin{aligned}
Q_{comp} &= -\frac{T}{\rho_f}\frac{\partial \rho_f}{\partial T}\left(\vec{u_f}\cdot\vec{\nabla}p\right) \\
Q_{shear} &= \eta\left[\left(\frac{\partial u_{fx}}{\partial z}\right)^2 + \left(\frac{\partial u_{fy}}{\partial z}\right)^2\right]
\end{aligned} \tag{16}$$

For the stationary problem in this study, the boundary conditions for the heat equations are the following. For the top and bottom surfaces ($\partial\Omega_t$ and $\partial\Omega_b$ in figure 5(b)), the temperature is set as the initial temperature T_0. For the other surfaces, $T = T_0$ if the fluid is oriented into the contact centre; otherwise, $k\frac{\partial T}{\partial n} = 0$.

The material properties are given in table 3.

Solid	Balls	Disc 1
Material	Steel	
Young's modulus E [GPa]	210	
Poisson's ratio v	0.3	
Thermal conductivity k [$^{W}/_{mK}$]	21 [64]	
Specific heat c_p [$^{J}/_{kgK}$]	470	
Density ρ [$^{kg}/_{m^3}$]	7850	
Fluid	SQ	BB
Thermal conductivity k [$^{W}/_{mK}$]	0.14	0.13
Specific heat c_p [$^{J}/_{kgK}$]	1040	2058

Table 3: Materiel properties of the contacting solids and lubricant thermodynamic properties.

2.5 Friction measurements

We performed the experimental measurements for BB and SQ with the ball on the disc tribometer Jerotrib at LaMCoS - INSA de Lyon. Friction data of BB has already been described in [37].

The same procedure was applied to SQ. Operating conditions were designed to minimize thermal heating during experiments. Fully flooded conditions were ensured by dipping the ball into the lubricant reservoir. The latter was thermostated at three different temperatures for each fluid 293K, 313K and 333K. The same material is used for the two solid bodies a 100Cr6 bearing steel ball against a 100Cr6 steel disc. SRR was widely varied in order to reach friction plateau and thermal regimes. The entrainment velocity u_e was chosen to induce a central film thickness of the order of 100 nm to ensure EHD conditions. The operating conditions of the new friction data measured on SQ are presented in section 3.

3 Results and discussion

3.1 Eyring stress characterisation

a Squalane

The confined NEMD simulations on SQ were carried out at four temperatures 293K, 313K, 353K and 373K, and pressures varying from 100MPa to 2000MPa. For a given pressure and temperature, at least six different sliding velocities are considered, corresponding to shear rates in the range $10^8 s^{-1} \sim 10^{10} s^{-1}$. At these shear rates, the simulation time (≥ 5 ns) is sufficient to bring the system to a steady state. In figure 6, shear stress versus shear rate data at 500MPa from this study are shown as an example. The

Eyring fit (equation 4(b)) used to derive the Eyring stress τ_e from the slope of the data is also marked by the dashed line. It must be noted that for each fit, the Newtonian viscosity η_N is fixed to the experimental values given in 2.2.b or, if necessary, to the value interpolated by the viscosity model. The only fitting parameter is τ_e. This can explain the slight discrepancy that can occur between the NEMD data and the fitting curve. This approach is however selected in order to derive an Eyring stress consistent with the Newtonian viscosity. It means that the pair of parameters (η_N, τ_e) represents the best fit of the NEMD data by an Eyring law (equation 4(b)), as it is drawn in dashed lines in Figure 6.

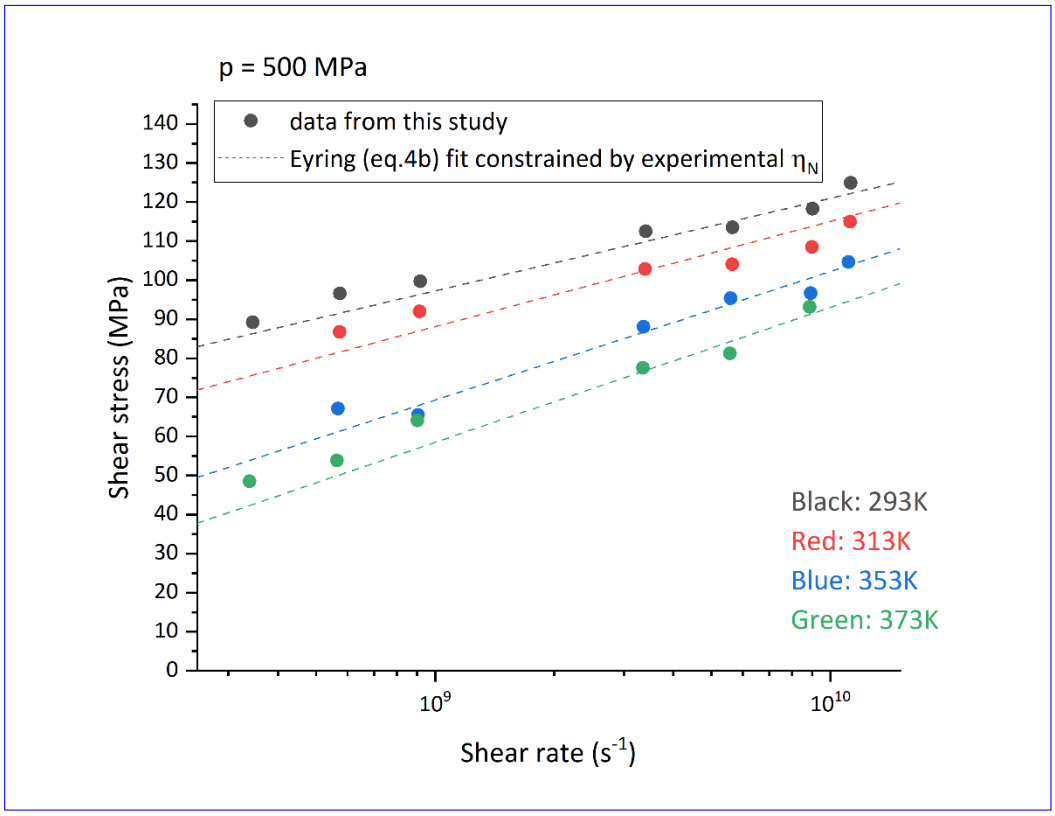


Figure 6: SQ shear stress at 500MPa. Dots stand for confined NEMD data calculated following the protocol described in 2.3. Dashed lines stand for the fit of the NEMD data by an Eyring law (equation 4(b). Different colours indicate different temperatures.

Figure 7 compares the τ_e results from this study and from the literature, including both bulk NEMD [40] and confined NEMD [14].

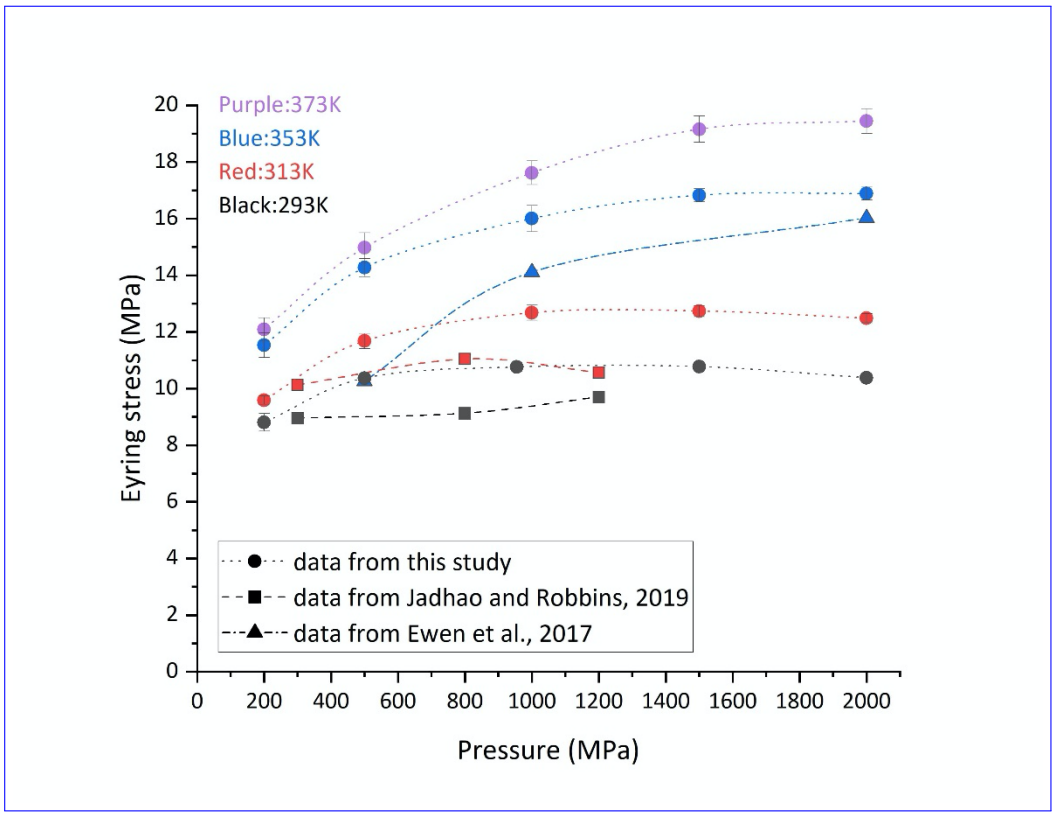


Figure 7: SQ Eyring stress. Comparison between results from this study (confined NEMD, dots and dot lines) and data from the literature Jadhao and Robbins [40] (bulk NEMD, squares and dash lines), Ewen et al. [14] (confined NEMD, triangles and dash-dot line). Different colours are used to indicate different temperatures.

Jadhao and Robbins [40] reported that τ_e could be independent of pressure for temperatures higher than 250K and pressures higher than 300MPa. On the other hand, Ewen et al. [14] and the present study reported data that showed a comparable variation of τ_e with pressure. The temperature dependency is well reproduced, although the present result overestimates τ_e when compared to [14] and [40]. Moreover, for SQ as a Group IV base oil (saturated hydrocarbons),this tendency of τ_e to increase with pressure was also observed recently by Zhang and Spikes [65] through tribology experiments.

The discrepancies may arise from differences between simulations. Ewen et al. [14] applied a Langevin thermostat inside the contact surfaces, which clearly had a limited ability to remove heat compared to the Nosé-Hoover thermostat set on all solids and fluids in the present study (see section 2.3). As Ewen et al. focused on comparing the NEMD results directly with the tribological experimental results, they had less interest in constraining the thermal effects in contact. They only thermostatted wall atoms to simulate the experimental thermal gradient development [66]. Instead, we attempted to characterise fluid property and construct a constitutive equation for p and T. This had to be done in an isothermal, isobaric environment. A larger temperature rise can thus be anticipated in the NEMD simulations of Ewen et al., causing a decrease of the shear stress and Eyring stress τ_e.

The SLLOD method used by Jadhao and Robbins [40] simulated 125 SQ molecules and used a united-atom (UA) force field to be able to reach low shear rates such as $10^5 s^{-1} \sim 10^6 s^{-1}$. In the present study only two orders of magnitude in shear rate is explored and a bigger system with 720 SQ molecules constrained by the all-atom (AA) force field is used to avoid layering caused by excessive confinement [18].

On the one hand, the reference work from Jadhao and Robbins, covering four orders of magnitude in rate, shows a substantial logarithmic behaviour of stress at high shear rate, compared to the present study where the Newtonian viscosity is fixed from equation 7. This may explain the higher Eyring stress values in the present work. On the other hand, when using a more coarse-grained model, the dynamics can be affected by the degree of coarse-graining, thus giving quantitative differences. In addition, the SLLOD method used by Jadhao and Robbins uses the NVT ensemble, whereas the confined NEMD method used in this study ensures pressure stability in the simulated system by applying constant pressure to the unfixed upper contact surface, similar to the NPT ensemble. This may also contribute to the observed difference.

For these reasons, only the data from the present MD simulations are used in the following. The variation of the Eyring stress of SQ τ_e^{SQ} with respect to pressure p [MPa] and temperature T [K] is shown in equation 17, which is implemented in the FEM contact model. The data used and the derived equation are shown in figure 8. It should be noted that this characteristic equation of τ_e^{SQ} is only valid in the range of tested p (100MPa to 2000MPa) and T (293K to 373K).

$$\tau_e^{SQ}[MPa] = A(T)\left(1 - \exp\left(-\frac{p}{B(T)}\right)\right) + C(T)$$
$$A(T) = a_1 * T + a_2 \qquad B(T) = b_1 * T + b_2 \qquad C(T) = c_1 * T + c_2 \tag{17}$$

a1 [MPa/K]	a2 [MPa]	b1 [MPa/K]	b2 [MPa]	c1 [MPa/K]	c2 [MPa]
0.0562	-10.3708	4.0035	-1001	0.0477	-9.2686

Table 4 Parameters of SQ Eyring stress equation.

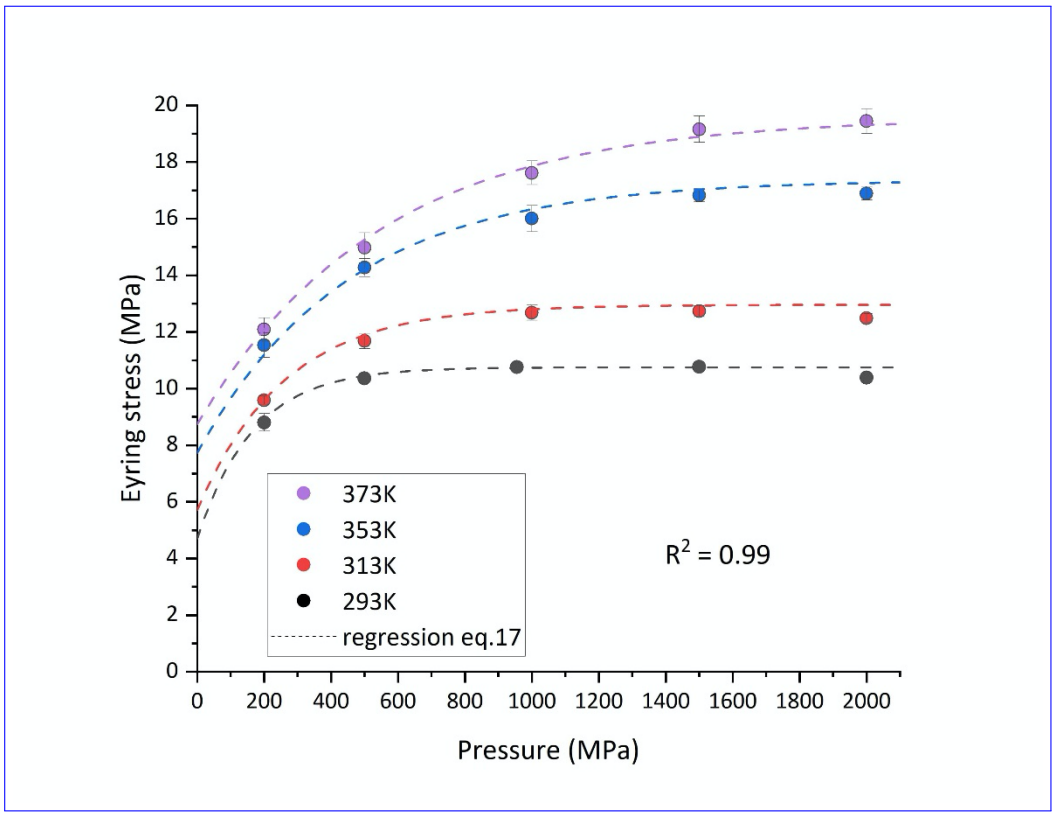


Figure 8 SQ Eyring stress from this study (symbols) and regression (dashed lines) as a function of pressure and temperature.

b Benzyl benzoate

The NEMD simulations were carried out on BB for temperatures ranging from 293K to 373K and pressures ranging from 200MPa to 1000MPa. For each pressure and temperature, at least seven sliding velocities were considered, corresponding to shear rates in the range of $10^{8}s^{-1} \sim 10^{10}s^{-1}$. Since BB has been less studied than SQ, no result from the literature could be found to support the present study. The simulation time was long enough (≥ 8ns) to ensure a steady-state situation. An example of shear stress versus shear rate data at 500MPa is shown in figure 9. The same Eyring fits as used on the SQ are applied and marked with dashed lines. The derived τ_e values are shown in figure 10.

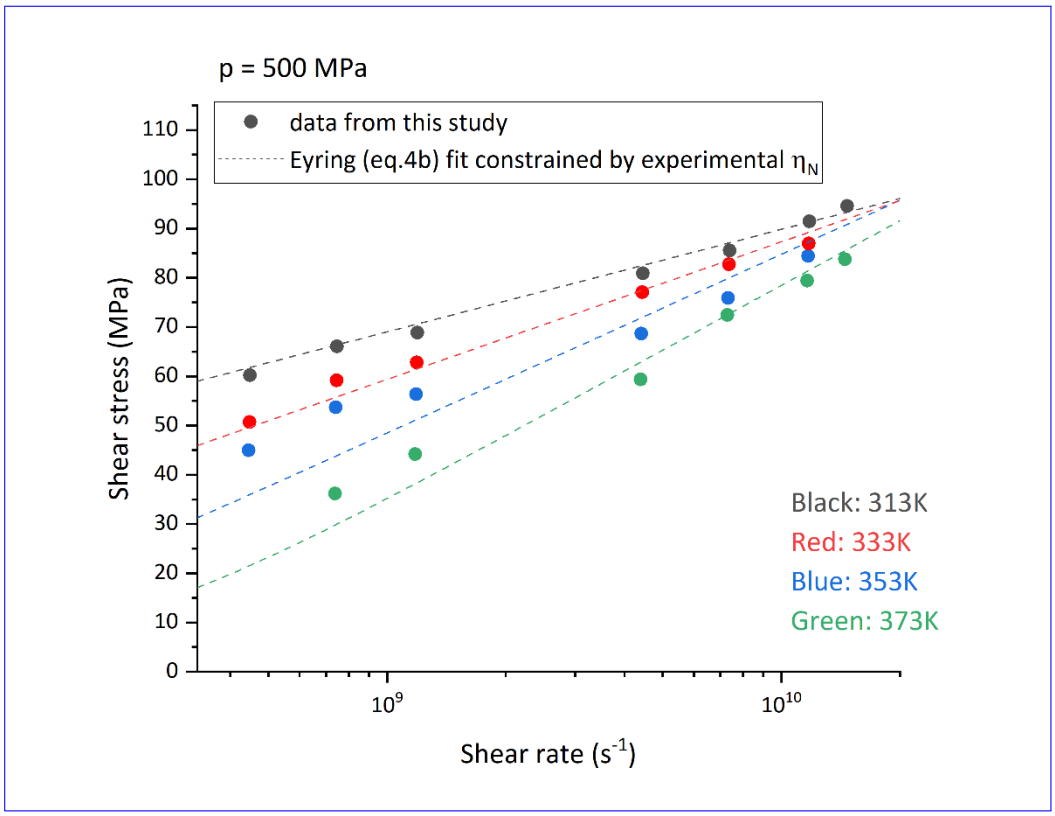


Figure 9 BB shear stress at 500MPa. Results from this study (confined NEMD, dots) and Eyring (equation 4(b)) fits used to calculate the Eyring stress are demonstrated. Different colours are used to indicate different temperatures.

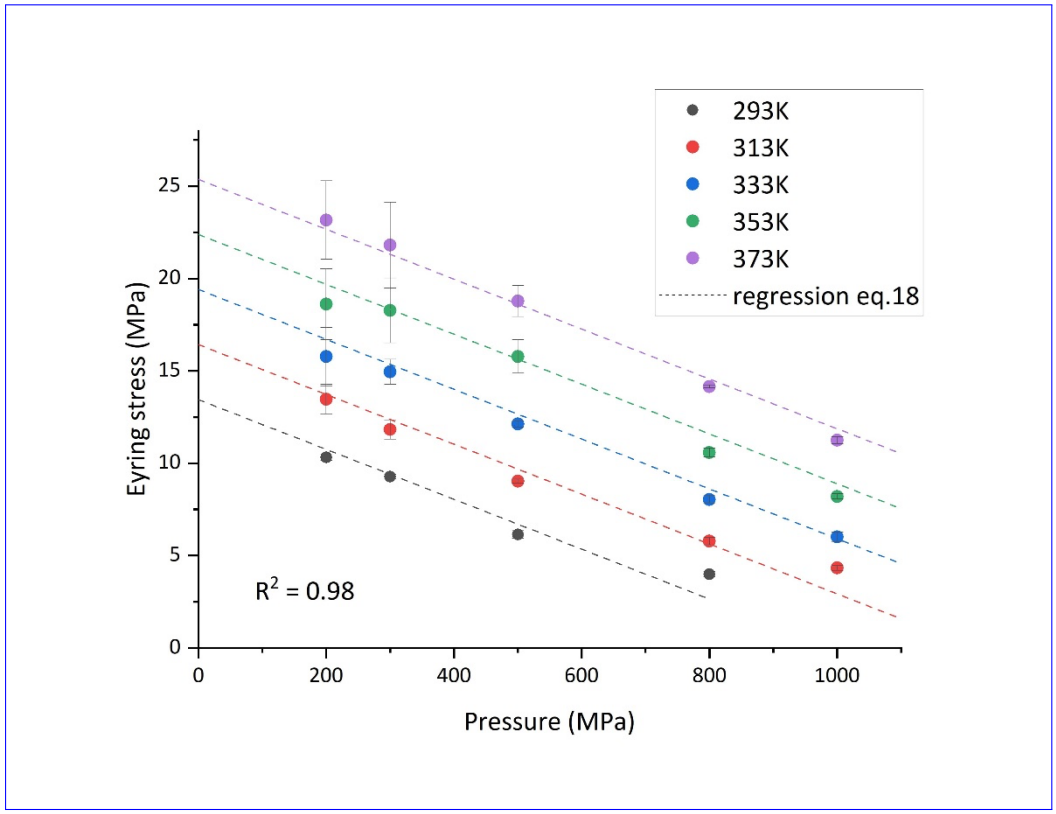


Figure 10 BB Eyring stress from this study (symbols) and linear regression (dashed lines) as a function of pressure.

Figure 10 shows that the Eyring stress of the BB, τ_e^{BB}, exhibits a rather simple dependency on pressure and temperature. It appears that τ_e^{BB} is inversely proportional to the pressure. A similar observation was made by Evans and Johnson [8] for another traction fluid, Santotrac 50. A linear regression of the results relates the τ_e^{BB} with pressure p[MPa] and temperature T[K], as shown in equation 18.

$$\tau_e^{BB}[MPa] = 0.149T - 0.014p - 30.21 \tag{18}$$

Similar to the case of SQ, the characteristic equation of τ_e^{BB} is only valid in the range of tested p (200MPa to 1000MPa) and T (293K to 373K). Since the Eyring stress cannot decrease to zero or even to a negative value as the pressure increases, we speculate that they will converge to a minimum value, an assumption that will be discussed in subsequent studies.

3.2 EHD friction prediction

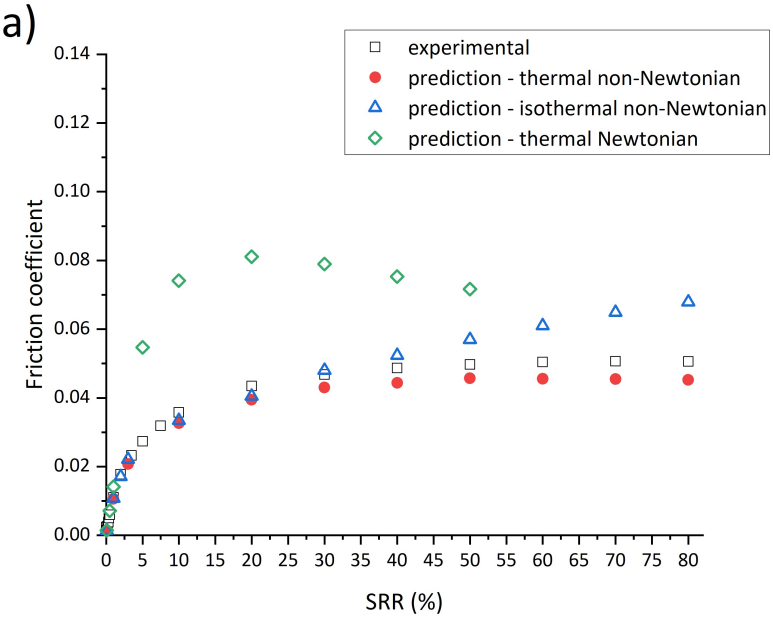
The full Eyring rheological model is established for both SQ and BB, with η_N given by the thermal scaling model based on experimentally measured viscosity and the characterisation of τ_e through MD simulations. It is then implemented into the TEHDnN contact model as described in section 2.4. The numerical simulations are carried out in the same operating conditions as the experiments, as shown in table 5, and results are compared with experimental friction measurement as explained in section 2.5.

Conditions	SQ	BB
Temperature [K]	313	313, 333
Contact load *w* [N]	46, 108, 254	32, 61
Max Hertzian pressure p_h [MPa]	900, 1200, 1600	800, 1000
Entrainment speed u_e [$^m/_s$]	0.8	2.5, 5
Slide to Roll Ratio SRR [%]	0.1-80	0.1-50

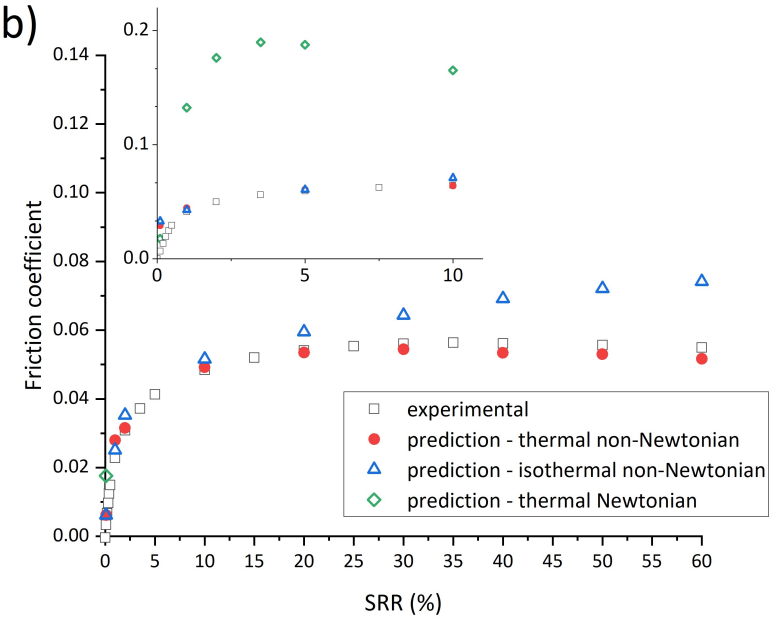
Table 5 Tribological experiment conditions of SQ and BB

Friction curves are shown in figure 11 and figure 12, where fig.11(a), (b), and (c) stand for SQ. Fig.12(a), (b), and (c) stand for BB.

(a)


experimental
prediction - thermal non-Newtonian
prediction - isothermal non-Newtonian
prediction - thermal Newtonian
Friction coefficient
SRR (%)

(b)


experimental
prediction - thermal non-Newtonian
prediction - isothermal non-Newtonian
prediction - thermal Newtonian
Friction coefficient
SRR (%)

(c)

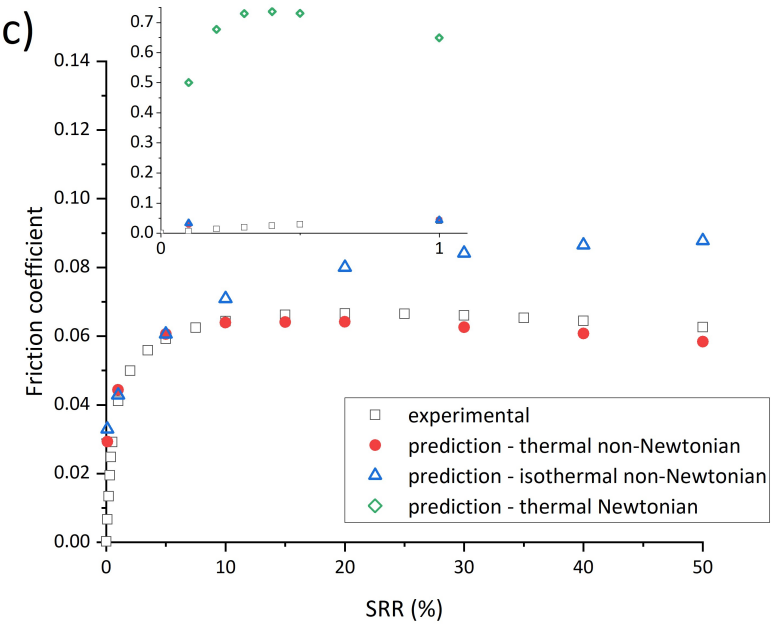

experimental
prediction - thermal non-Newtonian
prediction - isothermal non-Newtonian
prediction - thermal Newtonian
Friction coefficient
SRR (%)

Figure 11 Comparison between experimental measurements from this study (black squares) and prediction results of thermal non-Newtonian simulation (red dots), isothermal non-Newtonian simulation (blue triangles) and thermal Newtonian simulation (green diamond). (a) SQ 313K p_h=900MPa. (b) SQ 313K p_h=1200MPa. (c) SQ 313K p_h=1600MPa.

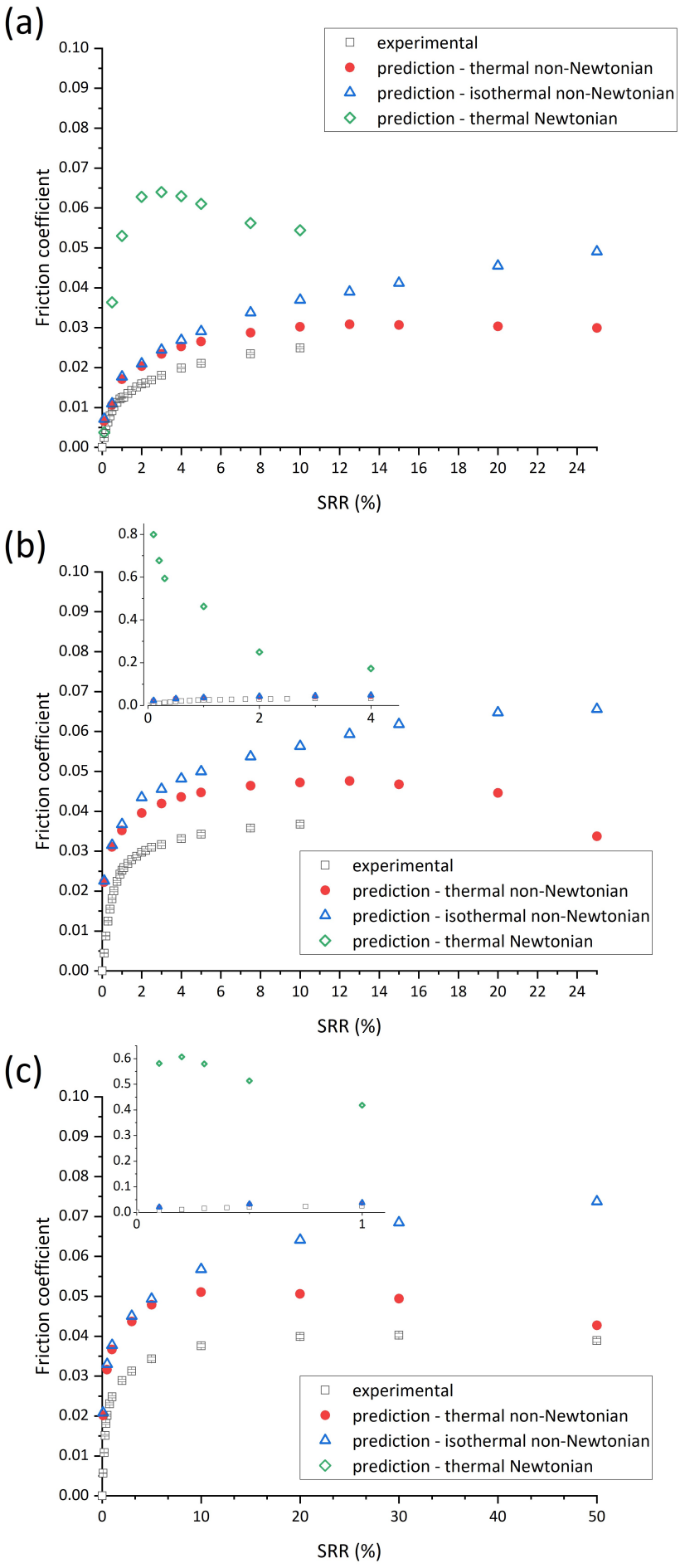

(a)
experimental
prediction - thermal non-Newtonian
prediction - isothermal non-Newtonian
prediction - thermal Newtonian
Friction coefficient
SRR (%)
(b)
experimental
prediction - thermal non-Newtonian
prediction - isothermal non-Newtonian
prediction - thermal Newtonian
Friction coefficient
SRR (%)
(c)
experimental
prediction - thermal non-Newtonian
prediction - isothermal non-Newtonian
prediction - thermal Newtonian
Friction coefficient
SRR (%)

Figure 12 Comparison between experimental measurements from [37] (black squares) and prediction results of thermal non-Newtonian simulation (red dots), isothermal non-Newtonian simulation (blue triangles) and thermal Newtonian simulation (green diamond). (a) BB 333K p_h=800MPa. (b) BB 333K p_h=1000MPa. (c) BB 313K p_h=800MPa.

In the case of SQ (figure 11), the mean absolute percentage error (MAPE, for SRR>1%), as well as the maximum error between the experimental values and TEHDnN predictions, are always less than 10%. Also, the simulations reproduced very well the friction curve's linear and shear thinning regimes. More interestingly, the simulation results successfully predicted friction plateau and the thermal thinning regime.

For BB (figure 12), compared to the experimental measurements, the TEHDnN predictions show a MAPE of 25% to 34%, and the maximum error is up to 60% in the last case (figure 12(c)) at SRR=5%. Despite being a less accurate prediction than that for SQ, the prediction still provides a suitable order of magnitude for the friction coefficient of BB and reproduces qualitatively the linear and shear thinning regimes, as well as the plateau regime (figure 12(a) and (b)) and the thermal thinning regime (figure 12(c)). It is also worth noting that for cases (a) and (b), the highest experimental SRR is 10%. We have extended the maximum SRR to 25% in simulations, and the results show the occurrence of the thermal thinning regime in both cases.

The most likely cause of the deviation is the accuracy of the viscosity equation, in other words, the accuracy of the two parameters of the Eyring equation the Newtonian viscosity at contact pressure and the Eyring stress. To further investigate this issue, additional simulations were performed. We found that Eyring stress laws have little effect on the prediction results when the same Newtonian viscosity law is used. For instance, two Eyring stress laws were tested for SQ first came from the results of Jadhao and Robbins [40] (which is only dependent on T, see figure 7), and equation 17 from this study (dependent on p and T), the results only show a difference in friction of around 5% while the difference in Eyring stress can reach 20%. This friction prediction approach does not appear to be highly sensitive to the value of the Eyring stress. Its accuracy depends more on the lubricant's Newtonian viscosity at contact pressure conditions. This might explain why predictions of SQ are better than those for BB SQ,

as a reference fluid for EHD contact studies, has been well studied, and numerous experimental data support a more accurate Newtonian viscosity law. On the other hand, BB is rarely studied in the literature and is supported by little experimental data. Furthermore, experimental studies based on pressure conditions of SQ are close to those applied in friction tests (see figure 3(a)). However, as shown in figure 3(b), the Newtonian viscosities of BB for tested contact conditions are far from the experimental measurement range and located within the extrapolation of the viscosity law. This difference also accounts for the prediction accuracy between the two fluids. In this perspective, quantitative friction prediction is a more significant challenge for this fluid, although it is the aim of the present strategy.

To be able to discuss in more detail the origin of friction plateau (LSS), the non-Newtonian effect, and the thermal effect need to be isolated. Consequently, two additional simulations are performed for each case and the results are also reported in figure 11 and 12. Isothermal non-Newtonian simulations prevent temperature rise due to heat generation. Thermal Newtonian simulations consider η_N as the viscosity instead of the Eyring model, avoiding the shear thinning.

Unsurprisingly, the thermal Newtonian simulations show a rapid linear rise of friction coefficient at very low SRR. Then due to the thermal effect, the friction slope gradually decreases with increasing SRR until it becomes negative (meaning that the thermal thinning in this friction regime has a more significant impact than the natural increase of shear stress with shear rate). The initial friction slope, as well as the maximum friction value, increase with pressure (figure 11(a), (b), (c) and figure 12(a), (b)) and decrease with temperature (figure 12(a), (c)) due to the evolution of the rheological properties with both parameters.

On the other hand, the isothermal non-Newtonian simulations consistently represent the experimental reference at low to moderate SRR (up to SRR = 20% for SQ and a significantly lower SRR value for BB). But they are unable to reproduce friction decrease at high SRR (figures 11(c) and figure 12(c)).

Three main remarks could be drawn from the previous results.

First, neither the thermal nor the non-Newtonian effects alone can reproduce the friction plateau observed experimentally. As a consequence, the friction plateau is due to a combined effect of shear thinning (non-Newtonian effect) and thermal thinning (thermal effect), and this is well reproduced by the TEHDnN simulation (figure 11 and 12).

Second, these new results reveal how the thermal effect changes friction. It is often thought that the impact of the thermal effect is more likely to be felt under relatively high SRRs, as shown in figure 1. However, this work shows that the thermal effects occur simultaneously with the shear thinning and continuously affect friction within the SRR range.

Finally, since the observed frictional plateau originates from a combination of thermal and non-Newtonian effects, empirical LSS laws are questionable and hardly reflect a general characterisation of the fluid. As an illustration, the thermal properties of the surfaces can influence thermal effects and thus the frictional response.

4 Conclusion

There is much research in the literature on the rheological properties of fluids and a large amount of research on experimental friction measurement in EHD contacts, but little work combines the two. The present study provides a new EHD friction prediction approach based on the Eyring viscosity model embedded in a finite element thermal-elastohydrodynamic contact model. This study tested two fluids of different natures, a typical lubricant, SQ and a traction fluid, BB.

The Eyring parameters of both fluids (the Newtonian viscosity η_N and Eyring stress τ_e) are first characterised using rheological measurement (η_N) and MD simulation (τ_e). With this contact independent data, the present approach quantitatively predicted the friction of experimental EHD contact. Different regimes for both fluids, including the plateau regime (LSS) and the thermal thinning regime, are very well reproduced. Compared with classical EHD friction prediction [23, 30, 33, 34], this approach does not require reference to any friction measurement. This makes it an important step towards the 'true' friction prediction and quantitative EHD lubrication [4].

In the present work, friction plateaus (LSS) in EHD contacts are shown to arise from a combination of thermal and non-Newtonian effects. This conclusion can be related to the variation of $\dot{\gamma}_{red.}$ in the contact. In fact, when the contact conditions change, the critical shear rate $\dot{\gamma}_c$ or the relaxation time $t_{rel} = 1/\dot{\gamma}_c$ also changes, consequently the $\dot{\gamma}_{red.}$ changes for the same SRR. Combined with the thermal effect, this determines friction under specific conditions. It may explain why friction plateaus tend to occur at higher contact pressures (for the same SRR) a lower critical shear rate (or longer relaxation time) due to high pressure makes it easier to reach high $\dot{\gamma}_{red.}$, and the higher viscosity also makes the thermal effect more pronounced. Furthermore, an assumption could be made based on these inferences that the occurrence of friction plateaus is generic. Since a sufficiently high $\dot{\gamma}_{red.}$ and a sufficiently strong thermal effect at a sufficiently high shear rate will eventually lead friction to drop. Although which of these two effects is in the dominant position in this process remains unclear because the results demonstrate that neither can independently reproduce the friction plateau observed in the experiment. In addition, this study also reveals how thermal effects affect EHD friction at low to moderate SRR and almost simultaneously with non-Newtonian effects.

Finally, based on these findings, demonstrating the versatility of this approach by using different contact surfaces and with simple or complex fluids is a possible future work. Besides, using pressure and temperature-dependent material properties, as stated by Habchi et al. [67], is a potential improvement of this approach.

5 Acknowledgements

The work was mainly supported by the INSA Lyon-SKF Research Chair “Lubricated Interfaces for the Future”. The authors acknowledge Scott Bair for the density measurement of benzyl benzoate under high pressure. The authors also thank the ANR for sponsoring the computing facilities of this work in the frame of the ANR-19-CE42-0002 project.

6 Conflict of interest

There is no conflict of interest.

References

[1] K. Holmberg, P. Andersson, and A. Erdemir, "Global energy consumption due to friction in passenger cars," *Tribology International*, vol. 47, pp. 221–234, 3 2012. [Online]. Available http//dx.doi.org/10.1016/j.triboint.2011.11.022

[2] D. C. Dowson and G. R. Higginson, *Elasto-hydrodynamic lubrication the fundamentals of roller and gear lubrication*. Pergamon Press, Oxford, 1966. [Online]. Available https//www.sciencedirect.com/science/article/pii/004316486790018X

[3] P. Vergne and S. Bair, "Classical EHL versus quantitative EHL A perspective part I real viscosity-pressure dependence and the viscosity-pressure coefficient for predicting film thickness," *Tribology Letters*, vol. 54, pp. 1–12, 2014.

[4] S. Bair, L. Martinie, and P. Vergne, "Classical EHL versus quantitative EHL A perspective part II — super-arrhenius piezoviscosity, an essential component of elastohydrodynamic friction missing from classical EHL," *Tribology Letters*, vol. 63, 9 2016.

[5] F. W. Smith, "Lubricant behaviour in concentrated contact systems - the castor oil-steel system," *Wear*, vol. 2, pp. 250–263, 1959.

[6] L. Martinie and P. Vergne, "Lubrication at extreme conditions A discussion about the limiting shear stress concept," *Tribology Letters*, vol. 63, 8 2016.

[7] R. Pit, H. Hervet, and L. Léger, "Direct experimental evidence of slip in hexadecane solid interfaces," *Physical Review Letters*, vol. 85, pp. 980–983, 2000.

[8] C. R. Evans and K. L. Johnson, "The rheological properties of elastohydrodynamic lubricants," *Proceedings of the Institution of Mechanical Engineers, Part C Journal of Mechanical Engineering Science*, vol. 200, pp. 303–312, 1986.

[9] B. Jacobson, "An experimental determination of the solidification velocity for mineral oils," *ASLE Transactions*, vol. 17, pp. 290–294, 1974.

[10] S. Bair and W. O. Winer, "A rheological model for elastohydrodynamic contacts based on primary laboratory data," *Journal of Tribology*, vol. 101, pp. 258–264, 1979. [Online]. Available http//www.asme.org/about-asme/terms-of-use

[11] M. Muraki, “Molecular structure of synthetic hydrocarbon oils and their rheological properties governing traction characteristics,” *Tribology International*, vol. 20, pp. 347–354, 1987.

[12] T. Tsubouchi, H. Hata, and Y. Yoshida, “Optimisation of molecular structure for traction fluids,” *Lubrication Science*, vol. 16, pp. 393–403, 2004.

[13] J. Zhang, A. Tan, and H. Spikes, “Effect of base oil structure on elastohydrodynamic friction,” *Tribology Letters*, vol. 65, pp. 1–24, 2017.

[14] J. P. Ewen, C. Gattinoni, J. Zhang, D. M. Heyes, H. A. Spikes, and D. Dini, “On the effect of confined fluid molecular structure on nonequilibrium phase behaviour and friction,” *Physical Chemistry Chemical Physics*, vol. 19, pp. 17883–17894, 2017.

[15] S. N. Ndiaye, “Ultimate behaviour of confined fluids under very high pressure and shear stress,” Ph.D. dissertation, INSA de Lyon, 2017. [Online]. Available https//tel.archives-ouvertes.fr/tel-02061350

[16] M. Alsaad, S. Bair, D. M. Sanborn, and W. O. Winer, “Glass transitions in lubricants Its relation to elastohydrodynamic lubrication (EHD),” *Journal of Tribology*, vol. 100, pp. 404–416, 7 1978. [Online]. Available https//asmedigitalcollection.asme.org/tribology/article/100/3/404/382589/Glass-Transitions-in-Lubricants-Its-Relation-to

[17] S. Ndiaye, L. Martinie, D. Philippon, M. Gonon-Caux, J. Margueritat, and P. Vergne, “On the influence of phase change in highly loaded frictional contacts,” *Tribology Letters*, vol. 68, pp. 1–23, 2020.

[18] A. Porras-Vazquez, L. Martinie, P. Vergne, and N. Fillot, “Independence between friction and velocity distribution in fluids subjected to severe shearing and confinement,” *Physical Chemistry Chemical Physics*, vol. 20, pp. 27280–27293, 2018.

[19] H. Spikes and Z. Jie, “History, origins and prediction of elastohydrodynamic friction,” *Tribology Letters*, vol. 56, pp. 1–25, 2014.

[20] K. L. Johnson and J. L. Tevaarwerk, “Shear behaviour of elastohydrodynamic oil films.” *Proc R Soc London Ser A*, vol. 356, pp. 215–236, 1977.

[21] C. R. Evans and K. L. Johnson, “Regimes of traction in elastohydrodynamic lubrication,” *Proceedings of the Institution of Mechanical Engineers, Part C Journal of Mechanical Engineering Science*, vol.

200, pp. 313–324, 9 1986. [Online]. Available http//journals.sagepub.com/doi/10.1243/PIME PROC 1986 200 135 02

[22] B. Jacod, C. H. Venner, and P. M. Lugt, "A generalized traction curve for EHL contacts," *Journal of Tribology*, vol. 123, pp. 248–253, 4 2001.

[23] B. Jacod and C. H. Venner and P. M. Lugt, "Extension of the friction mastercurve to limiting shear stress models," *Journal of Tribology*, vol. 125, pp. 739–746, 10 2003.

[24] A. V. Olver and H. A. Spikes, "Prediction of traction in elastohydrodynamic lubrication," *Proceedings of the Institution of Mechanical Engineers, Part J Journal of Engineering Tribology*, vol. 212, pp. 321–332, 5 1998. [Online]. Available http//journals.sagepub.com/doi/10.1243/1350650981542137

[25] G. E. Morales-Espejel and A. W. Wemekamp, "An engineering approach on sliding friction in full-film, heavily loaded lubricated contacts," *Part J J. Engineering Tribology*, vol. 218, 2004.

[26] W. Habchi, I. Demirci, D. Eyheramendy, G. Morales-Espejel, and P. Vergne, "A finite element approach of thin film lubrication in circular ehd contacts," *Tribology International*, vol. 40, pp. 1466–1473, 2007.

[27] W. Habchi, D. Eyheramendy, P. Vergne, and G. Morales-Espejel, "A full-system approach of the elastohydrodynamic line/point contact problem," *Journal of Tribology*, vol. 130, pp. 1–10, 4 2008.

[28] S. Bair, C. McCabe, and P. T. Cummings, "Calculation of viscous EHL traction for squalane using molecular simulation and rheometry," *Tribology Letters*, vol. 13, pp. 251–254, 2002.

[29] Y. Liu, Q. J. Wang, S. Bair, and P. Vergne, "A quantitative solution for the full shearthinning EHL point contact problem including traction," *Tribology Letters*, vol. 28, pp. 171–181, 11 2007.

[30] W. Habchi, D. Eyheramendy, S. Bair, P. Vergne, and G. Morales-Espejel, "Thermal elastohydrodynamic lubrication of point contacts using a newtonian/generalized newtonian lubricant," *Tribology Letters*, vol. 30, pp. 41–52, 4 2008.

[31] T. Doki-Thonon, "Thermal effects in elastohydrodynamic spinning circular contacts," Ph.D. dissertation, INSA de Lyon, 2012. [Online]. Available https//tel.archives-ouvertes.fr/tel-00749882

[32] J.-D. Wheeler, "Non-elliptical point contacts The torus-on-plane conjunction," Ph.D. dissertation, INSA de Lyon, 2016. [Online]. Available https//tel.archives-ouvertes.fr/ tel-01791538

[33] H. C. Liu, B. B. Zhang, N. Bader, C. H. Venner, and G. Poll, "Simplified traction prediction for highly loaded rolling/sliding EHL contacts," *Tribology International*, vol. 148, 8 2020.

[34] M. Björling, W. Habchi, S. Bair, R. Larsson, and P. Marklund, "Towards the true prediction of EHL friction," *Tribology International*, vol. 66, pp. 19–26, 2013. [Online]. Available http//dx.doi.org/10.1016/j.triboint.2013.04.008

[35] S. Bair and A. Laesecke, "Normalized ashurst-hoover scaling and a comprehensive viscosity correlation for compressed liquids," *Journal of Tribology*, vol. 134, 2012.

[36] S. Bair, "Reference liquids for quantitative elastohydrodynamics Selection and rheological characterization," *Tribology Letters*, vol. 22, pp. 197–206, 5 2006.

[37] S. N. Ndiaye, L. Martinie, D. Philippon, N. Devaux, and P. Vergne, "A quantitative frictionbased approach of the limiting shear stress pressure and temperature dependence," *Tribology Letters*, vol. 65, pp. 1–14, 12 2017.

[38] J. P. Ewen, D. M. Heyes, and D. Dini, "Advances in nonequilibrium molecular dynamics simulations of lubricants and additives," *Friction*, vol. 6, pp. 349–386, 12 2018.

[39] V. Jadhao and M. O. Robbins, "Probing large viscosities in glass-formers with nonequilibrium simulations," *Proceedings of the National Academy of Sciences of the United States of America*, vol. 114, pp. 7952–7957, 7 2017.

[40] Vikram Jadhao and Mark O. Robbins, "Rheological properties of liquids under conditions of elastohydrodynamic lubrication," *Tribology Letters*, vol. 67, pp. 1–20, 9 2019. [Online]. Available https//doi.org/10.1007/s11249-019-1178-3

[41] A. Gupta, H. D. Cochran, and P. T. Cummings, "Shear behavior of squalane and tetracosane under extreme confinement, iii. effect of confinement on viscosity," *Journal of Chemical Physics*, vol. 107, pp. 10335–10343, 12 1997. [Online]. Available http//aip.scitation.org/doi/10.1063/1.474173

[42] J. D. Moore, S. T. Cui, P. T. Cummings, and H. D. Cochran, "Lubricant characterization by molecular simulation," *AIChE Journal*, vol. 43, pp. 3260–3263, 12 1997. [Online]. Available https//onlinelibrary.wiley.com/doi/10.1002/aic.690431215

[43] S. Bair, P. Vergne, P. Kumar, G. Poll, I. Krupka, M. Hartl, W. Habchi, and R. Larsson, "Comment on "history, origins and prediction of elastohydrodynamic friction" by spikes and jie," *Tribology Letters*, vol. 58, 2015.

[44] P. J. Carreau, "Rheological equations from molecular network theories." *Trans Soc Rheol*, vol. 16, pp. 99–127, 1972.

[45] K. Yasuda, R. C. Armstrong, and R. E. Cohen, "Shear flow properties of concentrated solutions of linear and star branched polystyrenes," *Rheol. Acta*, vol. 20, pp. 163–178, 1981.

[46] S. Bair, "A rough shear-thinning correction for ehd film thickness," *Tribology Transactions*, vol. 47, pp. 361–365, 7 2004.

[47] H. Eyring, "Viscosity, plasticity, and diffusion as examples of absolute reaction rates," *The Journal of Chemical Physics*, vol. 4, pp. 283–291, 1936.

[48] S. Bair, "A traction (friction) curve is not a flow curve," *Lubricants*, vol. 10, 9 2022.

[49] A. T. Hayward, "Compressibility equations for liquids A comparative study," *British Journal of Applied Physics*, vol. 18, pp. 965–977, 7 1967. [Online]. Available https//iopscience.iop.org/article/10.1088/0508-3443/18/7/312

[50] S. K. Mylona, M. J. Assael, M. J. Comun˜as, X. Paredes, F. M. Gacin˜o, J. Fern´andez, J. P. Bazile, C. Boned, J. L. Daridon, G. Galliero, J. Pauly, and K. R. Harris, "Reference correlations for the density and viscosity of squalane from 273 to 473 k at pressures to 200 mpa," *Journal of Physical and Chemical Reference Data*, vol. 43, 3 2014.

[51] S. Bair, private communication, 7 2016.

[52] D. J. Evans and G. P. Morriss, "Nonlinear-response theory for steady planar couette flow," *Physical Review A*, vol. 30, pp. 1528–1530, 9 1984. [Online]. Available https//link.aps.org/doi/10.1103/PhysRevA.30.1528

[53] S. Plimpton, "Fast parallel algorithms for short-range molecular dynamics," *Journal of Computational Physics*, vol. 117, pp. 1–19, 3 1995. [Online]. Available https //linkinghub.elsevier.com/retrieve/pii/S002199918571039X

[54] A. P. Thompson, H. M. Aktulga, R. Berger, D. S. Bolintineanu, W. M. Brown, P. S. Crozier, P. J. in 't Veld, A. Kohlmeyer, S. G. Moore, T. D. Nguyen, R. Shan, M. J. Stevens, J. Tranchida, C. Trott, and S.

J. Plimpton, “Lammps - a flexible simulation tool for particlebased materials modeling at the atomic, meso, and continuum scales,” *Computer Physics Communications*, vol. 271, p. 108171, 2 2022.

[55] D. J. Evans and B. L. Holian, “The nose-hoover thermostat,” *The Journal of Chemical Physics*, vol. 83, pp. 4069–4074, 1985.

[56] J. P. Ewen, S. E. Restrepo, N. Morgan, and D. Dini, “Nonequilibrium molecular dynamics simulations of stearic acid adsorbed on iron surfaces with nanoscale roughness,” *Tribology International*, vol. 107, pp. 264–273, 3 2017.

[57] A. I. Jewett, Z. Zhuang, and J.-E. Shea, “Moltemplate a coarse-grained model assembly tool,” *Biophysical Journal*, vol. 104, p. 169a, 1 2013. [Online]. Available http//dx.doi.org/10.1016/j.bpj.2012.11.953

[58] A. I. Jewett, D. Stelter, J. Lambert, S. M. Saladi, O. M. Roscioni, M. Ricci, L. Autin, M. Maritan, S. M. Bashusqeh, T. Keyes, R. T. Dame, J.-E. Shea, G. J. Jensen, and D. S. Goodsell, “Moltemplate A tool for coarse-grained modeling of complex biological matter and soft condensed matter physics,” *Journal of Molecular Biology*, vol. 433, p. 166841, 5 2021.

[59] A. H. Larsen, J. J. Mortensen, J. Blomqvist, I. E. Castelli, R. Christensen, M. Du lak,
J. Friis, M. N. Groves, B. Hammer, C. Hargus, E. D. Hermes, P. C. Jennings, P. B. Jensen,J. Kermode, J. R. Kitchin, E. L. Kolsbjerg, J. Kubal, K. Kaasbjerg, S. Lysgaard, J. B. Maronsson, T. Maxson, T. Olsen, L. Pastewka, A. Peterson, C. Rostgaard, J. SchiØtz, O. Schu¨tt, M. Strange, K. S. Thygesen, T. Vegge, L. Vilhelmsen, M. Walter, Z. Zeng, and
K. W. Jacobsen, “The atomic simulation environment - a python library for working withatoms,” *Journal of Physics Condensed Matter*, vol. 29, 6 2017.

[60] P. Spijker, G. Anciaux, and J.-F. Molinari, “The effect of loading on surface roughness at the atomistic level,” *Computational Mechanics*, vol. 50, pp. 273–283, 9 2012.

[61] M. I. Mendelev, S. Han, D. J. Srolovitz, G. J. Ackland, D. Y. Sun, and M. Asta, “Development of new interatomic potentials appropriate for crystalline and liquid iron,” *Philosophical Magazine*, vol. 83, pp. 3977–3994, 12 2003.

[62] S. W. Siu, K. Pluhackova, and R. A. B¨ockmann, “Optimization of the opls-aa force field for long hydrocarbons,” *Journal of Chemical Theory and Computation*, vol. 8, pp. 1459–1470, 2012.

[63] Y. Peiran and W. Shizhu, “A generalized reynolds equation for non-newtonian thermal elastohydrodynamic lubrication,” *Journal of Tribology*, vol. 112, pp. 631–636, 10 1990. [Online]. Available https//asmedigitalcollection.asme.org/tribology/article/112/4/631/ 435009/A-Generalized-Reynolds-Equation-for-NonNewtonian

[64] T. Reddyhoff, A. Schmidt, and H. Spikes, “Thermal conductivity and flash temperature,” *Tribology Letters*, vol. 67, pp. 1–9, 2019. [Online]. Available http //dx.doi.org/10.1007/s11249-018-1133-8

[65] J. Zhang and H. Spikes, “Measurement of ehd friction at very high contact pressures,” *Tribology Letters*, vol. 68, 3 2020.

[66] R. Khare, J. de Pablo, and A. Yethiraj, “Molecular simulation and continuum mechanics study of simple fluids in non-isothermal planar couette flows,” *The Journal of Chemical Physics*, vol. 107, pp. 2589–2596, 8 1997.

[67] W. Habchi, P. Vergne, S. Bair, O. Andersson, D. Eyheramendy, and G. E. Morales-Espejel, “Influence of pressure and temperature dependence of thermal properties of a lubricant on the behaviour of circular tehd contacts,” *Tribology International*, vol. 43, pp. 1842–1850,
10 2010. [Online]. Available http//dx.doi.org/10.1016/j.triboint.2009.10.002